8608 *Biochemistry* **2010,** *49,* 8608–8617
DOI: 10.1021/bi100742w

BIOCHEMISTRY
including biophysical chemistry & molecular biology
Article

Structural and Functional Characterization of the Recombinant Human Mitochondrial Trifunctional Protein[†]

Benjamin Fould, Virginie Garlatti, Emmanuelle Neumann, Daphna Fenel, Christine Gaboriaud, and Gérard J. Arlaud*

Institut de Biologie Structurale Jean-Pierre Ebel, 41 rue Jules Horowitz, 38027 Grenoble Cedex 1, France

Received May 11, 2010; Revised Manuscript Received August 9, 2010

ABSTRACT: The α and β subunits of the human mitochondrial trifunctional protein (TFP), the multienzyme complex involved in fatty acid β-oxidation, were coexpressed in *Escherichia coli* and purified to homogeneity by nickel affinity chromatography. The resulting α/His-β construct was analyzed by gel filtration, sedimentation velocity, and electron microscopy, indicating a predominance of $\alpha_2\beta_2$ and $\alpha_4\beta_4$ complexes, with higher order oligomers. Electron microscopy indicated that the elementary species $\alpha_2\beta_2$ had overall structural similarity with its bacterial homologue. As shown by cosedimentation and surface plasmon resonance analyses, recombinant TFP interacted strongly with cardiolipin and phosphatidylcholine, suggesting that the natural complex associates with the inner mitochondrial membrane through direct interactions with phospholipids. Recombinant TFP displayed 2-enoyl-CoA hydratase (ECH), L-3-hydroxyacyl-CoA dehydrogenase (HACD), and 3-ketoacyl-CoA thiolase (KACT) activities, and ECH and HACD each reached equilibrium when the downstream enzymes (HACD and KACT, respectively) were made inactive, indicating feed-back inhibition. The KACT activity was optimal at pH 9.5, sensitive to ionic strength, and inhibited at concentrations of its substrate 3-ketohexadecanoyl-CoA >5 μM. Its kinetic constants (k_{cat} = 169 s^{-1}, K_m = 4 μM) were consistent with those determined previously on a purified porcine TFP preparation. Using different assays, trimetazidine, an efficient antiaginal agent, had no significant inhibitory effect on any of the three enzymatic activities of the recombinant TFP preparation, in contrast with other reports. This study provides the first detailed structural and functional characterization of a recombinant human TFP preparation and opens the way to in-depth analyses through site-directed mutagenesis.

Fatty acid β-oxidation is a major source of energy in organisms ranging from bacteria to higher eukaryotes, involving four successive reactions that repetitively remove acetyl-coenzyme A (acetyl-CoA)[1] segments from fatty-acyl-CoA derivatives (*1*). Mammals possess both peroxisomal and mitochondrial β-oxidation systems, the latter comprising soluble enzymes in the matrix and a multienzyme complex designated trifunctional protein (TFP), bound to the inner mitochondrial membrane and specific for long-chain fatty acids (*2*−*6*). The β-oxidation spiral involves four enzymatic activities, acyl-CoA dehydrogenase, 2-enoyl-CoA hydratase (ECH), L-3-hydroxyacyl-CoA dehydrogenase (HACD), and 3-ketoacyl-CoA thiolase (KACT), the last three being catalyzed by TFP (Figure 1). The mammalian TFP complex and its bacterial homologue termed fatty acid β-oxidation multienzyme (FOM) each comprise two types of subunits: α, which holds the ECH and HACD activities, and β, harboring the KACT activity (*4*, *6*−*8*). The three-dimensional structure of the *Pseudomonas fragi* FOM complex has been solved by X-ray crystallography (*9*), revealing an $\alpha_2\beta_2$ heterotetramer with an uneven ring architecture, the ECH, HACD, and KACT catalytic sites each facing a central cavity exposed to the solvent. From this structure, a detailed channelling mechanism was inferred, where the fatty acid tail pivots sequentially from the ECH to the HACD and KACT active sites (*9*).

As judged from kinetic analyses (*10*), it is likely that mammalian TFP complexes also operate by means of a channelling mechanism. Based on the sequence similarity with the *P. fragi* FOM, an $\alpha_2\beta_2$ homology model of the human TFP complex has been derived (*9*). Nevertheless, it is unclear from analyses performed on human and rat TFP complexes whether these have an $\alpha_2\beta_2$ or $\alpha_4\beta_4$ stoichiometry (*4*, *5*, *10*, *11*). In addition, compared to their bacterial counterparts, mammalian TFP complexes exhibit significant sequence insertions in both the α and β subunits, and the structural and functional implications of these insertions remain to be determined. Another unsolved question lies in the nature of the interaction(s) that allow(s) mammalian TFP complexes to associate with the inner mitochondrial membrane. Finally, it is unclear from previous reports whether trimetazidine, an effective antiaginal drug, exerts its beneficial effects by inhibiting the KACT component of TFP (*12*, *13*) or has no effect on this enzyme (*14*).

The objective of this study was to provide answers to these questions and to yield further insights into the structure and function of human TFP, with particular attention to its KACT activity. For this purpose, a rapid and reliable method for expression of human TFP in *Escherichia coli* has been established, and the

[†]This work was supported by the Commissariat à l'Energie Atomique, the Centre National de la Recherche Scientifique, and the Université Joseph Fourier, Grenoble.

*Corresponding author. Phone: 33 4 38 78 49 81. Fax: 33 4 38 78 54 94. E-mail: gerard.arlaud@ibs.fr.

[1]Abbreviations: CL, cardiolipin; CoA, coenzyme A; ECH, 2-enoyl-CoA hydratase; FOM, fatty acid β-oxidation multienzyme; HACD, L-3-hydroxyacyl-CoA dehydrogenase; KACT, 3-ketoacyl-CoA thiolase; NAD, β-nicotinamide adenine dinucleotide; trimetazidine, 1-(2,3,4-trimethoxybenzyl)piperazine; PC, phosphatidylcholine; TFP, trifunctional protein.

 Published on Web 09/08/2010

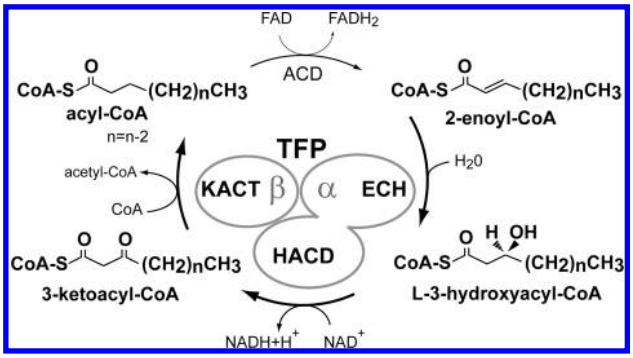

FIGURE 1: Schematic representation of the β-oxidation spiral. ACD, acyl-CoA dehydrogenase.

recombinant complex has been characterized using a variety of physicochemical and functional methods.

EXPERIMENTAL PROCEDURES

Reagents and Proteins. Restriction enzymes, $Vent_R$ polymerase, and alkaline phosphatase were obtained from New England Biolabs (Beverly, MA). The rapid DNA ligation kit was purchased from Roche. Antibiotics were obtained from Sigma-Aldrich and Euromedex. The pET-Duet expression vector and the *E. coli* strain Rosetta-2 (DE3) were obtained from Novagen. The DH5α *E. coli* strain was from Invitrogen. The His-select HF nickel affinity gel was purchased from Sigma-Aldrich.

3-Ketohexadecanoyl-CoA was obtained by chemical synthesis (Diverchim, Montataire, France). Briefly, (3-ketohexadecanoylsulfanyl)acetic acid was dissolved in 50 mM sodium tetraborate−HCl, pH 8.5, containing 50% *tert*-butyl alcohol and stirred under nitrogen for 4 h at 30 °C in the presence of 1.1 equiv of CoA trilithium salt. After decreasing the pH to 4.0 using perchloric acid, the reaction mixture was dried under vacuum. The residual white material was suspended in 1 volume of nitrogen-saturated water, adjusted to pH 1.0, mixed vigorously with 3 volumes of diethyl ether, cooled to 0 °C for 20 min to allow phase separation, and then centrifuged at 4000 rpm for 10 min at 4 °C. The white pellet was recovered, and the previous procedure was repeated five times to achieve complete elimination of residual reactants and byproduct. The purified 3-ketohexadecanoyl-CoA was freeze-dried and stored at −80 °C. Purity was typically >98%, as assessed by reverse-phase HPLC, using a method similar to that used for measuring KACT enzymatic activity. Identification was performed by ESI-TOF mass spectrometry, and quantification was done by weighing the freeze-dried compound.

2-Hexadecenoyl-CoA was synthesized enzymatically from hexadecanoyl-CoA using acyl-CoA oxidase and purified as described previously (*15*, *16*). Acyl-CoA oxidase from *Arthrobacter* sp., hexadecanoyl-CoA, β-nicotinamide adenine dinucleotide (NAD), coenzyme A, and tetradecanoyl-CoA were obtained from Sigma-Aldrich. Beef heart cardiolipin, egg yolk L-α-phosphatidylcholine type XVI, isopropyl 1-thio-β-D-galactopyranoside, and 1-(2,3,4-trimethoxybenzyl)piperazine (trimetazidine) were from Sigma-Aldrich. Octyl β-glucoside and all other detergents were obtained from Anatrace, and imidazole was from Fluka.

The concentrations of purified recombinant proteins were determined using absorption coefficients ($A_{1\%,1cm}$) at 280 nm estimated by the method of Edelhoch (*17*) and molecular weights calculated from the amino acid sequence as follows: TFP α, 0.4 and 79010; TFP His-β, 0.6 and 49309.

Construction of TFP α- and β-Containing Expression Plasmids. The following primers were obtained from Eurogentec (Seraing, Belgium) and used to amplify the desired human TFP sequences using $Vent_R$ polymerase, according to established procedures: CTAGTCATGAGCCATCACCATCACCATCACGAAAATCTGTATTTTCAGGGCACCAGAACCCATATTAAC (sense for His-α); TTTTCCTTTTGCGGCCGCTCACTGGTAGAACTTCTTGTTAGGGC (antisense for His-α); AGTCATTAATGCATCACCATCACCATCACGAAAATCTGTATTTTCAGGGCGCTGCCCCAGCTGTCC (sense for His-β); CCGCTCGAGTTATTTTGGATAAGCTTCC (antisense for His-β). The underlined sequences represent cleavage sites for *Bsp*HI, *Not*I, *Ase*I, and *Xho*I, respectively. The amplified His-α DNA (2.2 kbp) encoding the mature α subunit fused C-terminally to a hexahistidine tag and a TEV cleavage site was initially cloned into the pET-Duet multiple cloning site 1, between the *Bsp*HI and *Not*I sites. The corresponding His-β DNA (1.3 kbp) was then subsequently cloned into the multiple cloning site 2 of the vector, between the *Ase*I and *Xho*I sites, to yield the pET-Duet/His-α, His-β construct.

Deletion of the hexahistidine tag and TEV cleavage site on the N-terminal side of α to generate the pET-Duet/α, His-β construct was performed by PCR using the QuikChange XL site-directed mutagenesis kit (Stratagene, La Jolla, CA). The primer AAGGAGATATACCATGACCAGAACCCATATTAAC and its complementary sequence were used.

Deletion Mutants. The deletion mutants were generated by PCR using the QuikChange XL site-directed mutagenesis kit. The following primers and their complementary sequences were used: CCAACTGGTGGAACCCCTGGGATACCTAGAAGAAGTTGCAATTAC (mutant Δα1); CTGTATTTTCAGGGCAAACCCAATATAAGGAATGTTGTGGTGGTGG (mutant Δβ1); GTTGATGTCCGATGTGAGCATGATGCACGGTGTCGACCCTGCGGTTTCTG (mutant Δβ2); GGCAAATTTTAAAGCCATGGATTTGAGATTGCCTCCTGAGAAGTTTAATAACTGGGG (mutant Δβ3). All constructs were characterized by restriction mapping and checked by double-stranded DNA sequencing (Cogenics, Meylan, France).

Protein Production and Purification. The pET-Duet/α, His-β construct was integrated into the *E. coli* host strain Rosetta-2 (DE3). A 2 L culture was grown at 37 °C to an absorbance at 600 nm of 0.7−0.8. Protein production was then induced by addition of 0.1 mM isopropyl 1-thio-β-D-galactopyranoside and the culture incubated overnight at 23 °C. Cells were isolated by centrifugation and stored at −20 °C. After thawing, cells were suspended in 100 mM Tris-HCl, pH 8, and lysed by sonication for 6 min on ice, and the lysate was centrifuged at 22000*g* for 40 min. The supernatant was supplemented with 10 mM imidazole and 0.8% octyl β-glucoside and then loaded on a 5 mL His-select HF nickel affinity column. The column was washed with 100 mM Tris-HCl, 20 mM imidazole, and 0.8% octyl β-glucoside, pH 8.0, until the absorbance at 280 nm decreased below 0.05. The recombinant material was eluted using a linear 20−150 mM imidazole gradient, and the protein content was monitored by absorbance at 280 nm and SDS−PAGE analysis.

Chemical Analysis of the Recombinant Proteins. N-Terminal sequence analyses were performed after SDS−PAGE analysis and electrotransfer, using an Applied Biosystems model 477A protein sequencer as described previously (*18*). The electrospray ionization technique was used for mass spectrometry analysis of recombinant TFP, using an Agilent 1100 series HPLC coupled with an LC/MSD TOF mass spectrometer (Agilent).

All solvents were of HPLC grade. Protein samples were desalted with 0.03% formic acid in 66.5% acetonitrile using a Macro Trap cartridge (Michrom).

Gel Filtration Analysis. The recombinant TFP preparation was analyzed on a Superose 6 10/300 GL column (GE Healthcare), in 0.6% octyl β-glucoside and 100 mM Tris-HCl, pH 8.0, at a flow rate of 0.4 mL/min. *E. coli* β-galactosidase, rabbit muscle pyruvate kinase and lactate dehydrogenase, and horseradish peroxidase (Sigma-Aldrich) were used as molecular weight markers.

Analytical Ultracentrifugation. Sedimentation velocity analyses were performed using a Beckman XL-I analytical ultracentrifuge and an AN-60 TI rotor (Beckman Instruments, Fullerton, CA). Experiments were conducted at 10 °C in 100 mM Tris-HCl and 0.8% (w/v) octyl β-glucoside, pH 8.0. Samples (400 μL) were loaded into 12 mm path-length double-sector cells and centrifuged overnight at 42000 rpm. Absorbance at 280 nm was recorded. The sedimentation coefficients (s) were derived from the sedimentation velocity profiles using the Sedfitbeta program V11.72f (http://www.analyticalultracentrifugation.com), and the continuous distribution of sedimentation coefficients was obtained considering globular proteins. The solvent density and viscosity were measured at 1.005 g/mL and 1.332 cP, respectively. Partial specific volumes were estimated from the amino acid composition at 0.74 mL/g (α, $\alpha_2\beta_2$, and $\alpha_4\beta_4$) and 0.73 mL/g (β) using the Sednterp program (www.bbri.org/RASMB/rasmb.html).

Electron Microscopy. Recombinant TFP samples (10−100 μg/mL) were loaded on the clean side of carbon on mica (carbon/mica interface), negatively stained with 2% (w/v) sodium silicotungstate (pH 7.4), and air-dried. Micrographs were taken under low-dose conditions using a CM12 electron microscope (FEI, Eindhoven) operating at 120 kV. Images were collected with a SC1000 ORIUS TEM CCD camera (Gatan) with a pixel size of 1.5 Å. A total of 576 $\alpha_2\beta_2$ particles and 574 $\alpha_4\beta_4$ particles collected from nine images were selected for analysis using the X3D program (*19*). Raw images were filtered at 25 Å in order to enhance the contrast and then subjected to classification and averaging by means of the SPIDER software (*20*), using initially 46 projections of the FOM X-ray structure filtered at 25 Å as reference images. The resulting averaged images were next used to generate a model, and 46 projections of this model were used as new reference images for the alignment and classification process. A round of 20 similar cycles was performed to yield the final averaged images.

Cosedimentation Analyses. Large unilamellar vesicles containing phosphatidylcholine, cardiolipin, or a 10:1 molar ratio phosphatidylcholine:cardiolipin mixture were generated in 100 mM Tris-HCl, pH 8.0, at 10 mg/mL using a miniextruder (Avanti Polar Lipids) and a 0.1 μm polycarbonate membrane, according to the manufacturer's instructions (http://www.avantilipids.com). TFP samples (25−50 μg in 200 μL of 100 mM Tris-HCl, 0.2% octyl β-glucoside, pH 8.0) were incubated with each liposome (150 μg) for 30 min at 22 °C. Samples were centrifuged at 225000g for 30 min at 4 °C using a Beckman TLA-100.1 ultracentrifuge, allowing separation of the supernatant from the liposome-containing pellet. The protein contents of the supernatant and pellet fractions were determined by SDS−PAGE analysis followed by Coomassie blue staining.

Surface Plasmon Resonance Spectroscopy. Analyses were performed using a BIAcore X instrument (GE Healthcare). Cardiolipin vesicles were prepared as described above and loaded on an HPA sensor chip (GE Healthcare) as recommended by the manufacturer. The phospholipid-coated sensor chip was blocked with 0.1 mg/mL lipid-free bovine serum albumin. Binding of recombinant TFP (20−120 nM) was measured over 3500 resonance units of immobilized PC at a flow rate of 20 μL/min in 100 mM Tris-HCl, 50 mM NaCl, and 0.16% octyl β-glucoside, pH 8.0. Regeneration of the sensor chip surface was achieved by injection of 20 μL of 6 M guanidinium chloride.

Enzyme Assays. The 3-ketoacyl-CoA thiolase (KACT) activity of recombinant TFP was determined routinely from conversion of 3-ketohexadecanoyl-CoA to tetradecanoyl-CoA. The assay mixture contained 5 μM 3-ketohexadecanoyl-CoA, 1 mM CoA, and recombinant TFP in 100 mM Tris-HCl and 150 mM NaCl, pH 9.0. After incubation for 10 min at 37 °C, the reaction was stopped by addition of 33% acetonitrile. The mixture was analyzed by reverse-phase HPLC on a 3.9 × 150 mm Nova-Pak C18 column (Waters) by means of an Agilent series 1100 HPLC system, using a 14−56% linear acetonitrile gradient in 10 mM sodium tetraborate, pH 9.3, and detection at 259 nm. For determination of the kinetic constants of TFP, the concentrations of 3-ketohexadecanoyl-CoA ranged from 0.5 to 50 μM. The same HPLC-based assay was used to isolate the intermediate products of the β-oxidation reaction, using specific conditions as described in the legend to Figure 7.

Where indicated, the KACT activity was determined spectrophotometrically by monitoring the decrease in absorbance at 303 nm corresponding to the disappearance of the enolate form of 3-ketohexadecanoyl-CoA (*21*). The reaction mixture contained 10 μM 3-ketohexadecanoyl-CoA, 1 mM CoA, and recombinant TFP in 100 mM Tris-HCl, 50 mM KCl, and 25 mM $MgCl_2$, pH 8.0.

The combined 2-enoyl-CoA hydratase (ECH) and L-3-hydroxyacyl-CoA dehydrogenase (HACD) activities of TFP were measured by monitoring the conversion of NAD to NADH, as described by Fong and Schulz (*22*). The reaction mixture contained 30 μM 2-hexadecenoyl-CoA, 120 μM NAD, and recombinant TFP in 100 mM Tris-HCl, 100 mM KCl, and 0.1 mg/mL bovine serum albumin, pH 9.0, and the reaction was followed by the increase in absorbance at 340 nm.

Other Methods. SDS−PAGE and Western blot analyses were performed as described previously (*18*, *23*). Protein bands were revealed using antibodies raised against the human TFP α and β subunits expressed separately in *E. coli*.

RESULTS

Preliminary trials to separately express the α and β subunits of human TFP using a baculovirus/insect cells system resulted in the production of aggregated material carrying abnormal N-glycosylation(s) and devoid of KACT activity due to disulfide bridge formation in β, presumably between the Cys^{105} and Cys^{425} catalytic residues. Separate expression of the TFP subunits was then attempted using *E. coli* BL21(DE3)pLysS (Novagen), allowing production of α in a soluble form. In contrast, β was found to be poorly soluble, associated with the GroEL chaperone, and displayed only weak KACT specific activity (data not shown).

Expression and Purification of Recombinant TFP. In light of the above observations, we chose to perform coexpression of α and β in *E. coli*. For this purpose, both mature sequences fused to an N-terminal His tag were cloned into the pET-Duet vector. Of the various bacterial strains tested, Rosetta-2 (DE3) gave the highest yield and was therefore selected for protein

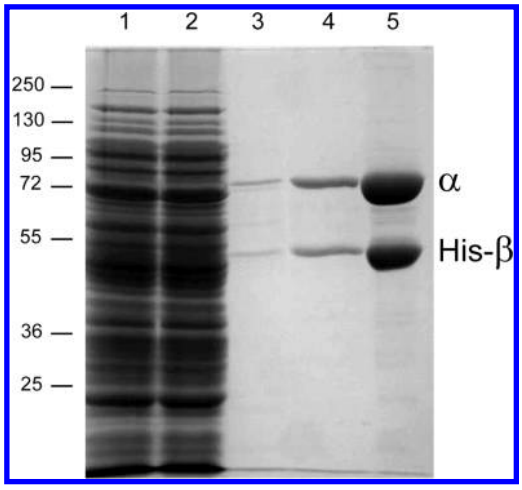

FIGURE 2: Purification of the recombinant TFP subunits. SDS−PAGE analysis: lane 1, whole bacterial lysate applied to the His-select HF nickel affinity column; lane 2, flow-through fraction; lane 3, fraction washed with 20 mM imidazole; lane 4, purified material eluted by the 20−150 mM imidazole gradient; lane 5, concentrated material. Analyses were performed under reducing conditions. The positions of the standard proteins are indicated.

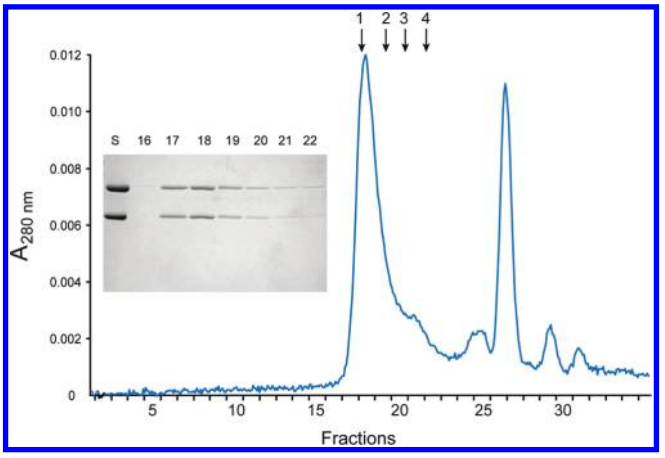

FIGURE 3: Gel filtration analysis of the recombinant TFP complex. The recombinant α/His-β complex was loaded on a Superose 6 column equilibrated in 0.6% octyl β-glucoside and 100 mM Tris-HCl, pH 8.0, at a flow rate of 0.4 mL/min. Fractions of 0.8 mL were collected. The elution positions of β-galactosidase (1), pyruvate kinase (2), lactate dehydrogenase (3), and peroxidase (4) are indicated. Insert: SDS−PAGE analysis under reducing conditions of the sample applied to the column (S) and fractions 16−22.

production. After comparative trials at varying temperatures and using different induction methods, optimal production of the recombinant proteins in a soluble form was achieved by induction with 0.1 mM isopropyl 1-thio-β-D-galactopyranoside and subsequent incubation overnight at 23 °C.

Purification of the recombinant His-α/His-β material was performed using a His-select HF nickel affinity column. The presence of a nonionic detergent such as octyl β-glucoside, Tween-20, Triton X-100, or Nonidet-P40 during the purification step was found to be necessary to achieve optimal protein recovery, and 0.8% octyl β-glucoside gave the best results in terms of purity. Nevertheless, preliminary analyses revealed that the purified material contained a large excess of α relative to β (data not shown). This led us to delete the His tag on α to allow purification of the α/β complex solely through the tag on β. Using the protocol described under Experimental Procedures, the average amount of purified material obtained in this way was about 2 mg/L of bacterial culture. As judged from SDS−PAGE analysis (Figure 2), this material was essentially pure and contained roughly equimolar amounts of α and His-β, with apparent molecular masses of 80 and 54 kDa, respectively. This provided a first indication of the ability of the recombinant α and His-β proteins to associate as a complex with a 1:1 stoichiometry. Both chains had identical electrophoretic mobilities under reducing and nonreducing conditions, indicative of the absence of disulfide bridges. The purified α/His-β complex could be concentrated up to 12 mg/mL in the presence of 0.8% octyl β-glucoside and remained stable for several weeks when stored at 0 °C.

Physicochemical Characterization of the Recombinant TFP Complex. N-Terminal sequence analysis of the recombinant TFP subunits after separation by SDS−PAGE yielded the following sequences: Thr-Arg-Thr-His-Ile-Asn-Tyr-Gly-Val-Lys-Gly-Asp-Val-Ala-Val... (α) and Met-His-His-His-His-His-His-Glu-Asn-Leu-Tyr-Gln-Gly-Ala-Ala-Pro... (His-β). The N-terminal residue of α is Thr^{37} of the nonmature sequence (*24*). The His-β sequence comprises the expected 6-His tag and the TEV cleavage site followed by the Ala-Ala-Pro sequence (positions 34−36 of the nonmature sequence), and is preceded by an extra Met residue arising from abnormal processing. Analysis by mass spectrometry yielded two sharp peaks with mass values of 79014 ± 40 Da (α) and 49291 ± 25 Da (His-β), in full agreement with the values of 79010 and 49309 Da calculated from the amino acid sequences. It was clear from the above analyses that both α and His-β had the expected primary sequences and exhibited no posttranslational modification.

The purified α/His-β complex was submitted to gel filtration analysis on a Superose 6 column in the presence of 0.6% octyl β-glucoside. As illustrated in Figure 3, most of the material was contained in a relatively sharp peak eluting in fractions 17−19, followed by a shoulder. Whereas no detectable protein was present in the following peaks as judged from SDS−PAGE analysis, this major species contained the α and His-β subunits, in a ratio of about 1.2:1, as determined by gel scanning, similar to the value determined for the starting material (Figure 3). Based on the relative elution positions of protein markers (see Experimental Procedures), the molecular mass of the complex contained in this major peak was estimated at about 460 kDa, a value in agreement with that determined for native TFP isolated from rat liver (*4*) and consistent with an $\alpha_4\beta_4$ complex (calculated mass 512 kDa). As judged from its elution position relative to protein markers, it appeared likely that the late eluting part of the major peak contained an $\alpha_2\beta_2$ species.

Analysis of the α/His-β complex by sedimentation velocity was performed as described under Experimental Procedures, yielding three major peaks 1−3 with sedimentation coefficients ($s_{20,w}$) of 10.4 ± 0.1, 15.6 ± 1, and 22.7 ± 1 S (Figure 4), and molecular masses calculated from S and D of 260 ± 10, 475 ± 75, and 820 ± 75 kDa, respectively. The first two values are fully compatible with $\alpha_2\beta_2$ and $\alpha_4\beta_4$ complexes, respectively, in good agreement with the gel filtration analysis. In contrast, the mass value of the third peak appears consistent with a larger species with an $\alpha_6\beta_6$ stoichiometry. This species was not observed by gel filtration analysis, suggesting that it was lost on the column.

Negative staining electron microscopy was next used to visualize the recombinant α/His-β material. As illustrated in Figure 5A, observation of the fraction contained in the major gel filtration peak revealed the presence of two types of particles differing in size and shape: (i) particles with an average diameter

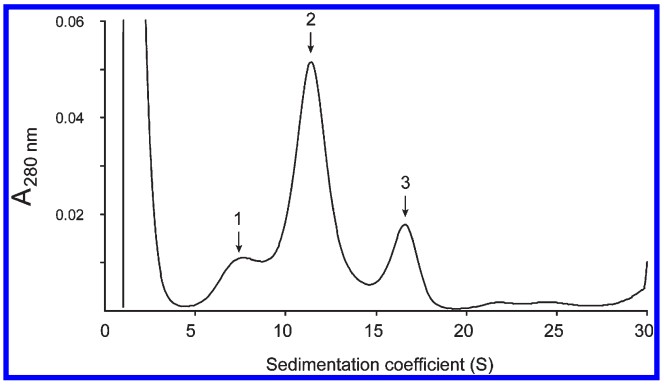

FIGURE 4: Sedimentation velocity analysis of the recombinant TFP complex. Analysis was performed as described under Experimental Procedures. Proteins were detected by monitoring absorbance at 280 nm. The continuous distribution of sedimentation coefficients is shown.

of about 12 nm, a size consistent with $\alpha_2\beta_2$ complexes, as judged from the *P. fragi* FOM X-ray structure (*9*), and (ii) larger particles (diameter 18 nm) likely corresponding, at least for the most part, to $\alpha_4\beta_4$ complexes.

From the images of the whole recombinant material, particles corresponding to the $\alpha_2\beta_2$ complex were selected and classified by means of the SPIDER software (*19*) (see Experimental Procedures). As filtered images of $\alpha_2\beta_2$ (Figure 5B1) were similar in size and shape to the FOM X-ray structure, projections of this structure (Figure 5B3) were initially used as reference images to perform this analysis. The final averaged images obtained after 20 iterative cycles (Figure 5B2) displayed high similarity to the FOM structure. The same procedure was also applied to the larger particles, yielding averaged images showing regularly shaped molecules comprising several domains, with overall dimensions consistent with an $\alpha_4\beta_4$ oligomeric state (Figure 5C).

Interaction with Phospholipids. Although the TFP complex is known to interact with the inner side of the inner mitochondrial membrane (*2*, *3*), the nature of this interaction remains to be elucidated. To investigate its ability to bind to phospholipids, the recombinant TFP complex was incubated with liposomes prepared from phosphatidylcholine, cardiolipin, or a phosphatidylcholine:cardiolipin mixture in a 10:1 molar ratio, mimicking the composition of the inner mitochondrial membrane (*25*). Interaction was assessed by cosedimentation analysis, from the relative amount of TFP associated with the vesicles in the ultracentrifugation pellet. As illustrated in Figure 6A, a large proportion of the TFP molecules bound to PC and PC/CL liposomes, and nearly complete binding was observed using liposomes containing pure CL. As judged from its ability to catalyze L-3-hydroxyacyl-CoA dehydrogenase activity (data not shown), the TFP complex remained fully functional in the presence of each liposome.

Further characterization of the TFP/CL interaction was achieved by surface plasmon resonance, using CL immobilized on an HPA sensor chip and recombinant TFP as the soluble ligand. The use of an HPA hydrophobic surface allows formation of a flat phospholipid monolayer with the polar groups oriented toward the fluid phase (*26*). As illustrated in Figure 6B, the TFP complex readily bound to CL monolayers, yielding curves with a very slow dissociation, indicative of a highly stable interaction. Indeed, efficient regeneration of the surface between two analyses could only be achieved using 6 M guanidinium chloride. Unfortunately, this treatment also detached a fraction of the

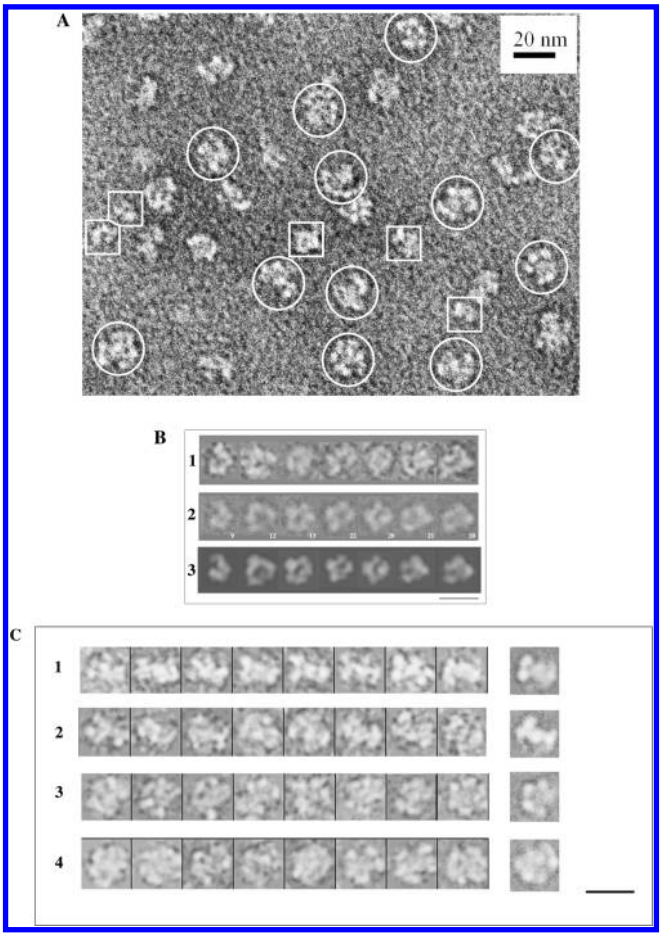

FIGURE 5: Negative-staining electron micrographs of the recombinant TFP complex. (A) Overall view of the fraction contained in the major gel filtration peak (Figure 3), highlighting the location of $\alpha_2\beta_2$ (squared) and $\alpha_4\beta_4$ (circled) particles. (B) Selected images of the $\alpha_2\beta_2$ particles: B1, raw images filtered at 25 Å resolution; B2, averaged images after alignment of the raw images against a set of reference images corresponding to different projections of the FOM X-ray structure (*9*) (PDB code 1WDK) (the number of raw particles in each class is indicated); B3, corresponding projections of the FOM X-ray structure filtered at 25 Å resolution. The scale bar represents 15 nm. (C) Selected images of the $\alpha_4\beta_4$ particles: C1−C4, four classes of raw images filtered at 25 Å. The average image corresponding to each class is shown on the right. The scale bar represents 21 nm.

immobilized CL, precluding accurate determination of the kinetic parameters of the interaction due to the lack of proportionality of the binding curves obtained at increasing TFP concentrations. Because of these technical problems, analysis of the interaction with PC monolayers was not attempted.

Recombinant TFP Displays ECH, HACD, and KACT Activities. Evidence that recombinant TFP exhibited both the ECH and HACD activities borne by the α subunit was obtained by monitoring conversion of NAD to NADH, using 2-hexadecenoyl-CoA as a substrate (data not shown). Based on NADH production, only about 40% of the product (3-ketohexadecanoyl-CoA) was formed in the absence of CoA, whereas addition of 1 mM CoA allowed the reaction to go to completion. Thus, full activity of the two enzymes characteristic of α could only be observed when the third enzyme, KACT, was functional.

The ability of recombinant TFP to catalyze *β*-oxidation of 2-hexadecenoyl-CoA was further dissected using reverse-phase HPLC (Figure 7), under conditions allowing the reactions to reach equilibrium. In the absence of both NAD and CoA, only the ECH activity was functional, leading to partial conversion of

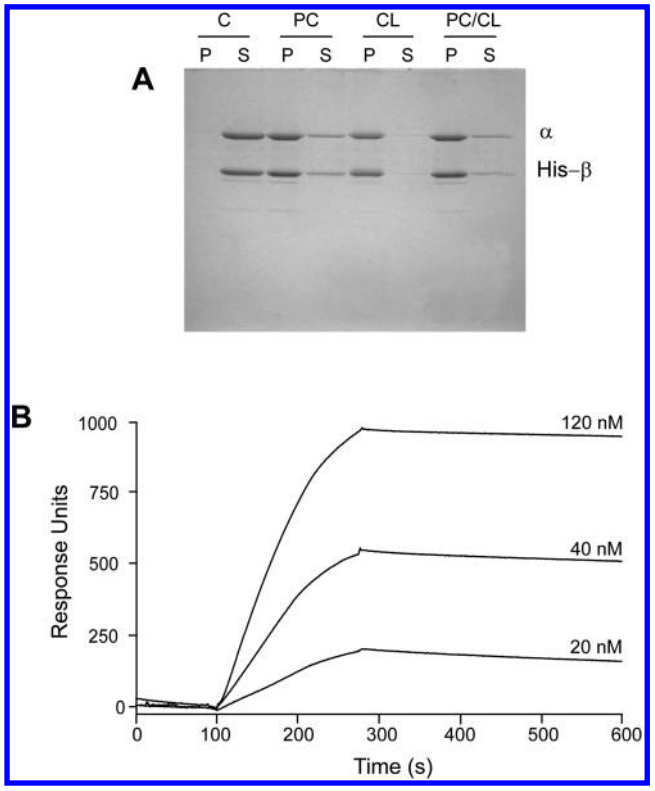

FIGURE 6: Interaction of recombinant TFP with phospholipids. (A) Cosedimentation analysis. TFP samples were incubated with different phospholipid vesicles and submitted to ultracentrifugation, and interaction was assessed by SDS−PAGE analysis of the supernatant and pellet fractions as described under Experimental Procedures. Key: C, negative control in the absence of vesicles; PC, CL, and PC/CL, vesicles containing PC alone, CL alone, or a 10:1 PC:CL mixture; P, pellet; S, supernatant. (B) Surface plasmon resonance analysis of the interaction between the recombinant TFP complex (20−120 nM) and immobilized PC (3500 resonance units).

2-hexadecenoyl-CoA to 3-hydroxyhexadecanoyl-CoA (Figure 7B). In the presence of NAD only, both the ECH and HACD activities were operative, leading to further consumption of 2-hexadecenoyl-CoA and 3-hydroxyhexadecanoyl-CoA and production of 3-ketohexadecanoyl-CoA (Figure 7C). Addition of both NAD and CoA enabled the whole β-oxidation spiral to be functional, allowing production of tetradecanoyl-CoA by KACT and resulting in almost complete consumption of the substrate and the intermediate products (Figure 7D). These observations provided clear evidence that recombinant TFP was enzymatically active and indicated that full ECH and HACD activities required the downstream enzyme (HACD and KACT, respectively) to be functional.

Characterization of the KACT Activity. The KACT activity of recombinant TFP was further characterized by means of the reverse-phase HPLC assay, using 3-ketohexadecanoyl-CoA as a substrate. As illustrated in Figure 8A, the enzyme activity was very weak at neutral pH and markedly increased above pH 7.5 to reach an optimal value at pH about 9.5. The influence of ionic strength was also investigated, showing that the KACT activity reached a plateau at 150 mM NaCl and progressively decreased at lower NaCl concentrations to reach about 30% of the optimal value in the absence of NaCl. Similar results were obtained using KCl.

To determine the kinetic constants for the KACT activity of recombinant TFP, the enzyme activity was assayed at 3-ketohexadecanoyl-CoA concentrations ranging from 0.5 to 50 μM.

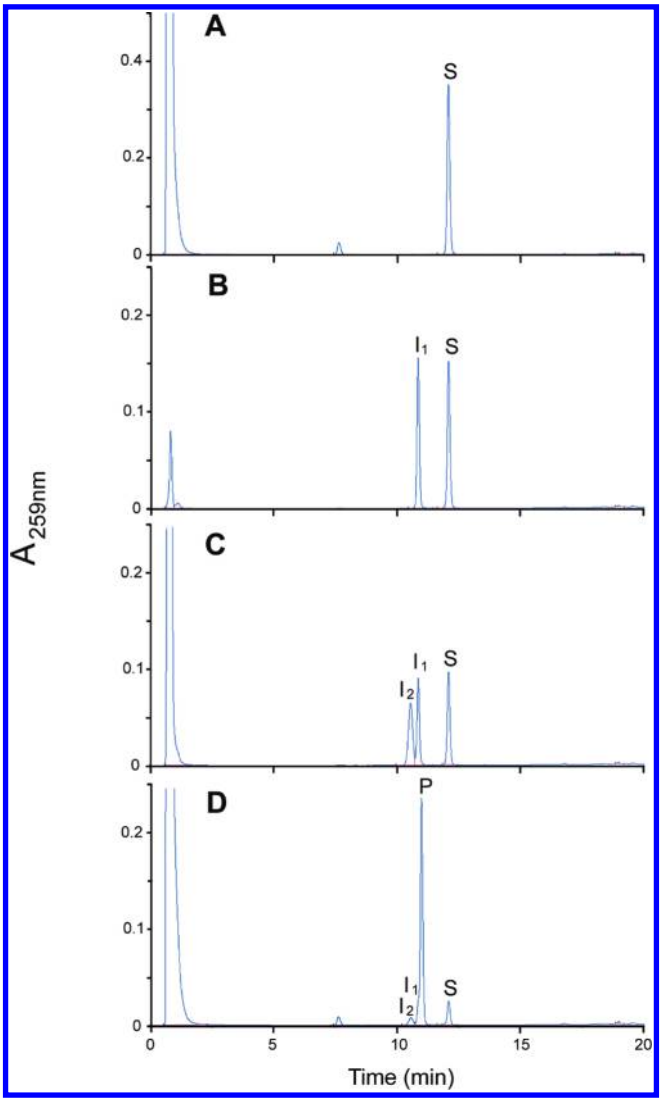

FIGURE 7: Reverse-phase HPLC analysis of the β-oxidation of 2-hexadecenoyl-CoA catalyzed by recombinant TFP. All samples contained 30 μM 2-hexadecenoyl-CoA in 100 mM Tris-HCl, 100 mM KCl, and 0.1 mg/mL bovine serum albumin, pH 9.0, and were incubated for 10 min at 37 °C. (A) Control sample lacking TFP. (B) Sample containing 1.3 μg of TFP. (C) Sample containing TFP + 120 μM NAD. (D) Sample containing TFP + NAD + 1 mM CoA. Reactions were stopped by addition of 33% acetonitrile, and analyses were carried out by reverse-phase HPLC using the solvent system described under Experimental Procedures for determination of the KACT activity. Key: S, 2-hexadecenoyl-CoA; I_1, 3-hydroxyhexadecanoyl-CoA; I_2, 3-ketohexadecanoyl-CoA; P, tetradecanoyl-CoA.

As best illustrated in the double-reciprocal representation (Figure 8B), increasing the substrate concentration above 5 μM resulted in progressive inhibition of the KACT activity, indicative of inhibition by excess substrate. The kinetic constants determined for the KACT activity of recombinant TFP are listed in Table 1. Although the k_{cat} is at first sight much higher than that reported for a native porcine TFP preparation (*10*), this latter value was derived from assays performed at pH 7.6 and in the absence of salt. Based on our own data, it is therefore likely to be greatly (about 20-fold) underestimated. In contrast, our k_{cat} and K_m values are both strikingly different from those reported by Liu et al. (*12*) for recombinant rat TFP.

Effect of Trimetazidine. To investigate its effect on the enzymatic activity of TFP, 50 or 100 μM trimetazidine was initially incubated with recombinant TFP for 30 min at room

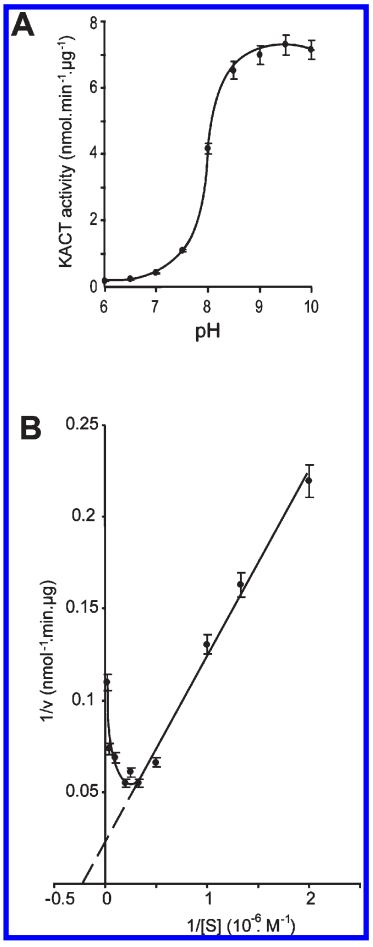

FIGURE 8: Characterization of the KACT activity of recombinant TFP: pH dependence and inhibition by excess substrate. (A) Variation of the KACT activity as a function of pH. Recombinant TFP was incubated for 10 min at 37 °C in the presence of 5 μM 3-ketohexadecanoyl-CoA, 1 mM CoA, and 50 mM KCl in a buffer containing 20 mM glycine and 30 mM acetic acid (pH adjusted to 6.0−10.0 by addition of Tris). (B) Double-reciprocal plot of the KACT activity as a function of substrate concentration. Recombinant TFP was incubated for 10 min at 37 °C in the presence of 0.5−50 μM 3-ketohexadecanoyl-CoA, 1 mM CoA, 150 mM NaCl, and 100 mM Tris-HCl, pH 9.0. The enzymic activity was determined in both cases using the reverse-phase HPLC assay as described under Experimental Procedures. The data shown represent the mean ± SD of three measurements.

Table 1: Catalytic Constants of the KACT Activity of Recombinant Human TFP

preparation	k_{cat} (s^{-1})	K_m (μM)	k_{cat}/K_m ($10^6\ s^{-1}\cdot M^{-1}$)
human TFP (recombinant)[a]	169 ± 26	4 ± 0.9	45 ± 12
porcine TFP (purified)[b]	8[c]	8.4	1
rat TFP (recombinant)[d]	641 ± 128[e]	51 ± 11	13 ± 4[e]

[a]This study. [b]From Yao and Schulz (*10*). [c]Value underestimated due to the nonoptimal assay conditions used. [d]From Liu et al. (*12*). [e]Values expressed relative to $\alpha_2\beta_2$.

temperature, and the residual KACT activity was determined using the reverse-phase HPLC assay. As shown in Figure 9, trimetazidine had no detectable inhibitory effect under these conditions, in contrast to iodoacetamide, a known inhibitor of thiolases (*27*). Identical results were obtained after overnight incubation at 4 °C (data not shown). Further analyses were conducted under strictly the same experimental conditions as used previously by Liu et al. (*12*),

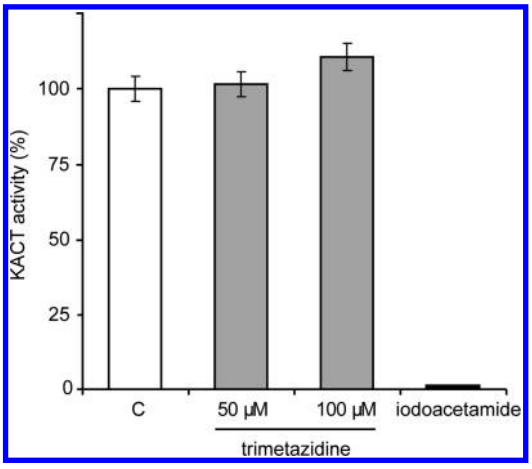

FIGURE 9: Effect of trimetazidine on the KACT activity of recombinant TFP. Recombinant TFP (4 ng) was incubated for 30 min at room temperature in the presence of 50 or 100 μM trimetazidine, and residual KACT activity was determined using the reverse-phase HPLC assay as described under Experimental Procedures. Key: C, control sample incubated in the absence of trimetazidine; iodoacetamide, negative control incubated with 5 mM iodoacetamide. The data shown represent the mean ± SD of three measurements.

including the spectrophotometric assay described under Experimental Procedures (*21*). Again, no inhibition of the KACT activity was detected upon incubation at room temperature or at 37 °C in the presence of 50 or 100 μM trimetazidine (data not shown). We also tested the effect of trimetazidine on the ECH and HACD activities harbored by the α subunit, using the spectrophotometric assay based on the conversion of NAD to NADH. Again, no inhibitory effect could be detected, indicating that the three enzymic activities of TFP were insensitive to trimetazidine.

Expression and Characterization of Deletion Mutants. To investigate the role of the four sequence insertions of TFP relative to its *P. fragi* FOM homologue, each of these insertions was individually deleted by PCR. The boundaries of the deleted segments were designed on a 3-D structural basis, taking into account the structural constraints imposed by the FOM structure (*9*), the derived TFP homology model (*9*), and the structures of homologous monofunctional enzymes, such as the human peroxisomal thiolase (E. Papagrigoriou et al., unpublished results; PDB code 2IIK). The single insertion of α (α1) was deleted by removing the ^{227}Pro−Thr^{236} segment (nonmature sequence numbering), thereby directly connecting Gly^{226} to Ile^{237}. The N-terminal extension of β (β1) was removed by excising the segment extending from Ala^{34} to Ala^{48}, thereby creating a new N-terminus Lys^{49}. In the case of β2, the large TFP segment extending from Val^{171} to Leu^{211} was replaced by the corresponding stretch ^{128}Val-Ser-Met-Met-His-Gly-Val-Asp^{135} from the FOM sequence. As for β3, the TFP segment ^{395}Ser−Leu^{414} was deleted and replaced by the shorter loop ^{360}Leu-Arg-Leu-Pro-Pro^{364} from the human peroxisomal thiolase.

Variants of the α/His-β construct carrying a single deletion in either α or β were produced recombinantly, and their overall expression levels as well as their solubility were compared to that of the wild-type construct (Figure 10). Deletion Δα1 did not significantly modify expression of α but greatly decreased its solubility. Interestingly, this also resulted in a decreased solubility of β, providing direct evidence that interaction with α is necessary to achieve full stability of this subunit. Deletions Δβ1 and Δβ2 each heavily decreased expression of β but had no impact on the expression and solubility of α, demonstrating that, in contrast to

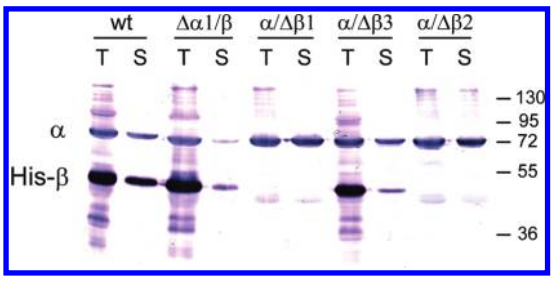

FIGURE 10: Expression and solubility of deletion mutants of TFP. The wild-type α/His-β construct and variants carrying mutations Δα1, Δβ1, Δβ2, or Δβ3 were produced. Cells were lysed in 100 mM Tris-HCl and 250 mM NaCl, pH 8, and the soluble fraction was recovered by centrifugation for 15 min at 10000*g*, as described (*38*). Key: T, total amount of material present in each cell lysate; S, soluble fraction recovered after centrifugation (samples were analyzed by SDS−PAGE under reducing conditions, followed by Western blot analysis using antibodies directed against α and β); wt, wild-type α/His-β construct; Δα1/β, α/Δβ1, α/Δβ2, and α/Δβ3, α/His-β constructs carrying deletion of insertions α1, β1, β2, or β3, respectively.

β, α is fully stable and soluble in the absence of β. In contrast, deletion Δβ3 had no effect on the expression level of β but greatly diminished its solubility. Since α was produced in a soluble form, this provided indirect evidence for an implication of loop β3 in the α/β interaction. Consistent with this hypothesis, purification of the α/Δβ3 construct on the nickel affinity column allowed us to recover low amounts of β but showed no evidence for the presence of α (data not shown). Further analysis of the variants carrying the Δα1, Δβ1, and Δβ2 mutations could not be performed due to the low amounts of soluble material available.

DISCUSSION

We have used coexpression in *E. coli* Rosetta-2 (DE3) to produce the recombinant α and His-β subunits of the human TFP complex. The single His tag fused to β allowed both recombinant proteins to bind to a nickel affinity column, providing evidence of their ability to associate to each other and allowing us to purify the α/His-β complex to homogeneity. In contrast, preliminary attempts to separately express the TFP subunits in *E. coli* did not allow production of β in a soluble form. Indeed, subsequent analysis of the solubility of α/His-β variants carrying deletions on α or β (see Figure 10) provided additional evidence that, whereas α is stable and soluble in the absence of β, β itself only acquires full stability upon interaction with α, hence the requirement for coexpressing the two subunits. These findings are in line with a previous report on the *P. fragi* FOM complex expressed in *E. coli* (*28*) indicating that, whereas the isolated α subunit exhibits both the ECH and HACD activities, β alone lacks KACT activity. In sharp contrast with the above observations, the β subunit of rat TFP expressed alone in *E. coli* as a fusion with Mistic, a bacterial integral membrane protein used for membrane protein expression (*29*, *30*), was reported to retain KACT activity (*12*). However, it seems likely that, owing to its large size (13 kDa), the Mistic fusion protein possibly conceals hydrophobic areas of β, thereby improving its solubility and/or stability in the absence of α. Our preliminary observation that β expressed alone in *E. coli* is associated with the GroEL chaperone appears to be consistent with this hypothesis.

As judged from the gel filtration, sedimentation velocity, and electron microscopy analyses performed in this study, the recombinant α/His-β complex is present in two major forms, $\alpha_2\beta_2$ and $\alpha_4\beta_4$, with lower amounts of a larger species possibly corresponding to a higher oligomer $\alpha_6\beta_6$. As shown by the electron microscopy images, the heterotetrameric $\alpha_2\beta_2$ complex has an overall architecture homologous to that determined by X-ray crystallography for the *P. fragi* FOM complex (*9*), indicating that α and β have similar folds and associate in similar ways in both cases. The key issue is to determine whether the native TFP complex found in its natural context corresponds to this species $\alpha_2\beta_2$ or to one of the higher oligomers observed in the present study. On one hand, given its structural similarity with its bacterial homologue, the elementary $\alpha_2\beta_2$ TFP species is expected to be functional, and therefore the need for a higher oligomeric species appears to be questionable. These species could therefore represent artifactual assemblies of the $\alpha_2\beta_2$ complex formed *in vitro*, possibly due to the lack of interaction with the inner mitochondrial membrane. Such a tendency to oligomerize *in vitro* would reconcile previous conflicting studies reporting that the purified human and rat TFP complexes have $\alpha_2\beta_2$ and $\alpha_4\beta_4$ stoichiometries, respectively (*4*, *5*). On the other hand, it should be emphasized that the larger $\alpha_4\beta_4$ particles seen in the electron microscopy images (Figure 5A) appear to be structured and regularly shaped, suggesting that they do not result from random aggregation. In addition, the fact that the α and β subunits of human TFP exhibit sequence insertions relative to their bacterial counterparts raises the possibility that some of them could mediate interactions between the elementary $\alpha_2\beta_2$ species. Thus, the possibility that the native form of human TFP is an oligomer of the elementary unit $\alpha_2\beta_2$ cannot be excluded, and further investigations at the cellular level are required to resolve this issue.

Analyses by cosedimentation and surface plasmon resonance provide conclusive evidence that the recombinant TFP complex interacts with phosphatidylcholine and cardiolipin, two phospholipids characteristic of the inner mitochondrial membrane. Although the kinetic constants of the interaction with immobilized cardiolipin monolayers could not be accurately determined, the K_D was roughly estimated to be in the low nanomolar range, indicating very strong interaction. This suggests that TFP could associate with the inner mitochondrial membrane through direct interactions with phosphatidylcholine or cardiolipin, or both, without the implication of a posttranslational modification, considering that both the α and His-β subunits expressed in this study have the predicted mass. Nevertheless, it cannot be excluded that binding to cardiolipin allows TFP to form a supercomplex with a putative protein partner, as shown for complexes III and IV of the mitochondrial respiratory chain (*31*). The very long chain acyl-CoA dehydrogenase, the enzyme that catalyzes the initial step of the β-oxidation spiral, would be a good candidate for this purpose. That one or more of the extra loops of α and/or β mediate interactions with the phospholipids, in a manner similar to that described for the sarcomeric mitochondrial creatine kinase (*25*) or the very long chain acyl-CoA dehydrogenase (*32*), appears likely.

The various enzymatic assays performed in this study provide clear evidence of the ability of the recombinant TFP material to perform the last three reactions of the β-oxidation spiral. As stated above, the kinetic constants measured for the KACT activity appear to be consistent with those determined by Yao and Schulz (*10*) on a purified porcine TFP preparation, taking into account that these authors did not use optimal assay conditions. In contrast, our values are strikingly different from those reported by Liu et al. (*12*) for recombinant rat TFP. Although this discrepancy remains to be explained, this could arise in part from the fact that different assays were used to

measure KACT activity. Alternatively, this could reflect species differences, despite the high sequence analogy between the rat and human proteins (*24*, *33*).

The basic optimal pH determined for the KACT activity of our recombinant TFP preparation is in line with the value of 9.0 reported for the combined ECH/HACD activities of purified human TFP (*16*). Nevertheless, given that the matrix pH of a respiring mitochondria is about 8 (*34*), this would imply that the KACT activity of TFP is not optimal in its natural environment. The fact that slight pH changes on either side of this value result in considerable variations of activity (Figure 8A) suggests a possible pH-dependent regulation. From a general standpoint, it should be emphasized that, due the amphiphilic nature of 3-ketohexadecanoyl-CoA, both pH and ionic strength are expected to modify its critical micelle concentration (*35*). Thus, the variations of KACT activity observed in each case are likely to result from effects on both the enzyme and the substrate.

Whereas all three enzymatic activities of recombinant TFP went to completion when both NAD and CoA were present, ECH and HACD each reached equilibrium when the downstream enzyme in the β-oxidation spiral (HACD and KACT, respectively) was made inactive through the lack of its cofactor (Figure 7). It is tempting to hypothesize that this effect arises from the channeling mechanism itself (*9*). In this hypothesis, however, the ECH and HACD reactions would be blocked at a very early stage, given the very low amount of TFP used (about 5 pM) relative to the substrate concentration (30 μM). An alternative explanation is that both enzymes are subject to a negative feedback by their respective reaction product. This hypothesis appears likely, considering that comparable competitive inhibitions by the reaction products have been described for homologous monofunctional enzymes ECH (*36*) and HACD (*37*).

The inhibition of KACT activity observed at concentrations of its substrate 3-ketohexadecanoyl-CoA above 5 μM may be a consequence of the formation of micelles (*34*), hampering proper accommodation of the substrate in the active site. However, this effect could also be inherent in the channeling mechanism, considering that the substrate for KACT is expected to be transferred from HACD in a stepwise manner, not to be made available to the enzyme active site at high concentration (*9*).

In view of the conflicting reports on the effect of trimetazidine on the KACT activity of TFP (*12*−*14*), we have carefully investigated this question using different enzymatic assays, and these all concur in the conclusion that trimetazidine has no significant inhibitory effect on any of the three enzymatic activities of recombinant TFP, including KACT. This finding was unexpected, particularly in view of the recent report that trimetazidine irreversibly inhibits the KACT activity of recombinant rat TFP expressed in *E. coli* (*12*). We have no clear explanation for this discrepancy, considering that, in our hands, negative results were obtained in all cases, including when using strictly the same experimental conditions as described by these authors.

This study provides a rapid and appropriate method to produce the recombinant human TFP complex in a stable and fully active form, allowing the first thorough investigation of its structural and functional characteristics and opening the way to further in-depth analyses through the generation of site-directed point mutants.

ACKNOWLEDGMENT

We are grateful to Dr. Momoyo Ishikawa from the Biomolecular Engineering Research Institute, Osaka, for providing the homology model of human TFP. We thank Aline Appourcheaux and Christine Ebel for performing ultracentrifugation analyses, Izabel Bérard for performing mass spectrometry measurements, Nicole Thielens for advice about molecular biology protocols, and Guy Schoehn for helpful discussions.

REFERENCES

1. Kim, J.-J. P., and Battaile, K. P. (2002) Burning fat: the structural basis of fatty acid β-oxidation. *Curr. Opin. Struct. Biol. 12*, 721–728.
2. Sumegi, B., and Srere, P. A. (1984) Binding of the enzymes of fatty acid beta-oxidation and some related enzymes to pig heart inner mitochondrial membrane. *J. Biol. Chem. 259*, 8748–8752.
3. Carpenter, K., Middleton, B., and Pollitt, R. J. (1991) The long-chain 3-hydroxyacyl-CoA dehydrogenase of human liver mitochondria. *J. Inherited Metab. Dis. 14*, 321–324.
4. Uchida, Y., Izai, K., Orii, T., and Hashimoto, T. (1992) Novel fatty acid beta-oxidation enzymes in rat liver mitochondria. II. Purification and properties of enoyl-coenzyme A (CoA) hydratase/3-hydroxyacyl-CoA dehydrogenase/3-ketoacyl-CoA thiolase trifunctional protein. *J. Biol. Chem. 267*, 1034–1041.
5. Carpenter, K., Pollitt, R. J., and Middleton, B. (1992) Human liver long-chain 3- hydroxyacyl-coenzyme A dehydrogenase is a multifunctional membrane-bound beta-oxidation enzyme of mitochondria. *Biochem. Biophys. Res. Commun. 183*, 443–448.
6. Luo, M. J., He, X.-Y., Sprecher, H., and Schulz, H. (1993) Purification and characterization of the trifunctional beta-oxidation complex from pig heart mitochondria. *Arch. Biochem. Biophys. 304*, 266–271.
7. Binstock, J. F., Pramanik, A., and Schulz, H. (1977) Isolation of a multi-enzyme complex of fatty acid oxidation from *Escherichia coli*. *Proc. Natl. Acad. Sci. U.S.A. 74*, 492–495.
8. Imamura, S., Ueda, S., Mizugaki, M., and Kawaguchi, A. (1990) Purification of the multienzyme complex for fatty acid oxidation from *Pseudomonas fragi* and reconstitution of the fatty acid oxidation system. *J. Biochem. 107*, 1193–1199.
9. Ishikawa, M., Tsuchiya, D., Oyama, T., Tsunaka, Y., and Morikawa, K. (2004) Structural basis for channelling mechanism of a fatty acid beta-oxidation multienzyme complex. *EMBO J. 23*, 2745–2754.
10. Yao, K. W., and Schulz, H. (1996) Intermediate channeling on the trifunctional beta-oxidation complex from pig heart mitochondria. *J. Biol. Chem. 271*, 17816–17820.
11. Orii, K. E., Aoyama, T., Souri, M., Jiang, L. L., Orii, K. O., Hayashi, S., Yamaguchi, S., Kondo, N., Orii, T., and Hashimoto, T. (1996) Formation of the enzyme complex in mitochondria is required for function of trifunctional beta-oxidation protein. *Biochem. Biophys. Res. Commun. 219*, 773–777.
12. Liu, X., Wu, L., Deng, G., Li, N., Chu, X., Guo, F., and Li, D. (2008) Characterization of mitochondrial trifunctional protein and its inactivation study for medicine development. *Biochim. Biophys. Acta 1784*, 1742–1749.
13. Kantor, P. F., Lucien, A., Kozak, R., and Lopaschuk, G. D. (2000) The antianginal drug trimetazidine shifts cardiac energy metabolism from fatty acid oxidation to glucose oxidation by inhibiting mitochondrial long-chain 3-ketoacyl coenzyme A thiolase. *Circ. Res. 86*, 580–588.
14. MacInnes, A., Fairman, D. A., Binding, P., Rhodes, J. A., Wyatt, M. J., Phelan, A., Haddock, P. S., and Karran, E. H. (2003) The antianginal agent trimetazidine does not exert its functional benefit via inhibition of mitochondrial long-chain 3-ketoacyl coenzyme A thiolase. *Circ. Res. 93*, e26–e32.
15. Eaton, S., Pourfarzam, M., and Bartlett, K. (1996) The effect of respiratory chain impairment of beta-oxidation in rat heart mitochondria. *Biochem. J. 319*, 633–640.
16. Eaton, S., Middleton, B., and Bartlett, K. (1998) Control of mitochondrial beta-oxidation: sensitivity of the trifunctional protein to [NAD^+]/[NADH] and [acetyl-CoA]/[CoA]. *Biochim. Biophys. Acta 1429*, 230–238.
17. Pace, C. N., Vajdos, F., Fee, L., Grimsley, G., and Gray, T. (1995) How to measure and predict the molar absorption coefficient of a protein. *Protein Sci. 4*, 2411–2423.
18. Rossi, V., Gaboriaud, C., Lacroix, M., Ulrich, J., Fontecilla-Camps, J. C., Gagnon, J., and Arlaud, G. J. (1995) Structure of the catalytic region of complement protease C1s: study by chemical cross-linking and three-dimensional homology modeling. *Biochemistry 34*, 7311–7321.
19. Conway, J. F., and Steven, A. C. (1999) Methods for reconstructing density maps of "single" particles from cryoelectron micrographs to subnanometer resolution. *J. Struct. Biol. 128*, 106–118.

20. Frank, J., Radermacher, M., Penczek, P., Zhu, J., Li, Y., Ladjadj, M., and Leith, A. (1996) SPIDER and WEB: processing and visualisation of images in 3D electron microscopy and related fields. *J. Struct. Biol. 116*, 190–199.
21. Miyazawa, S., Osumi, T., and Hashimoto, T. (1980) The presence of a new 3-oxoacyl-CoA thiolase in rat liver peroxisomes. *Eur. J. Biochem. 103*, 589–596.
22. Fong, J. C., and Schulz, H. (1981) Short-chain and long-chain enoyl-CoA hydratases from pig heart muscle. *Methods Enzymol. 71*, 390–398.
23. Rossi, V., Bally, I., Thielens, N. M., Esser, A. F., and Arlaud, G. J. (1998) Baculovirus-mediated expression of truncated modular fragments from the catalytic region of human complement serine protease C1s. Evidence for the involvement of both complement control protein modules in the recognition of the C4 protein substrate. *J. Biol. Chem. 273*, 1232–1239.
24. Kamijo, T., Aoyama, T., Komiyama, A., and Hashimoto, T. (1994) Structural analysis of cDNAs for subunits of human mitochondrial fatty acid beta-oxidation trifunctional protein. *Biochem. Biophys. Res. Commun. 199*, 818–825.
25. Schlattner, U., Gehring, F., Vernoux, N., Tokarska-Schlattner, M., Neumann, D., Marcillat, O., Vial, C., and Wallimann, T. (2004) C-terminal lysines determine phospholipid interaction of sarcomeric mitochondrial creatine kinase. *J. Biol. Chem. 279*, 24334–24342.
26. Saenko, E., Sarafanov, A., Ananyeva, N., Behre, E., Shima, M., Schwinn, H., and Josic, D. (2001) Comparison of the properties of phospholipid surfaces formed on HPA and L1 biosensor chips for he binding of the coagulation factor VIII. *J. Chromatogr. A 921*, 49–56.
27. Middleton, B. (1974) The kinetic mechanism and properties of the cytoplasmic acetoacetylcoenzyme A thiolase from rat liver. *Biochem. J. 139*, 109–121.
28. Ishikawa, M., Mikami, Y., Usukura, J., Iwasaki, H., Shinagawa, H., and Morikawa, K. (1997) Reconstitution, morphology and crystallization of a fatty acid beta-oxidation multienzyme complex from *Pseudomonas fragi*. *Biochem. J. 328*, 815–820.
29. Roosild, T. P., Greenwald, J., Vega, M., Castronovo, S., Riek, R., and Choe, S. (2005) NMR structure of Mistic, a membrane-integrating protein for membrane protein expression. *Science 307*, 1317–1321.
30. Roosild, T. P., Vega, M., Castronovo, S., and Choe, S. (2006) Characterization of the family of Mistic homologues. *BMC Struct. Biol. 6*, 10.
31. Zhang, M., Mileykovskaya, E., and Dowhan, W. (2002) Gluing the respiratory chain together. Cardiolipin is required for supercomplex formation in the inner mitochondrial membrane. *J. Biol. Chem. 277*, 43553–43556.
32. McAndrew, R. P., Wang, Y., Mohsen, A.-W., He, M., Vockley, J., and Kim, J.-J. P. (2008) Structural basis for substrate fatty acyl chain specificity: crystal structure of human very long-chain acyl-CoA dehydrogenase. *J. Biol. Chem. 283*, 9435–9443.
33. Kamijo, T., Aoyama, T., Miyazaki, J., and Hashimoto, T. (1993) Molecular cloning of the cDNAs for the subunits of rat mitochondrial fatty acid beta-oxidation multienzyme complex. Structural and functional relationships to other mitochondrial and peroxisomal beta-oxidation enzymes. *J. Biol. Chem. 268*, 26452–26460.
34. Llopis, J., McCaffery, J. M., Miyawaki, A., Farquhar, M. G., and Tsien, R. Y. (1998) Measurement of cytosolic, mitochondrial, and Golgi pH in single living cells with green fluorescent proteins. *Proc. Natl. Acad. Sci. U.S.A. 95*, 6803–6808.
35. Constantinides, P. P., and Steim, J. M. (1985) Physical properties of fatty acyl-CoA. Critical micelle concentrations and micellar size and shape. *J. Biol. Chem. 260*, 7573–7580.
36. He, X. Y., Yang, S. Y., and Schulz, H. (1992) Inhibition of enoyl-CoA hydratase by long chain L-3-hydroxyacyl-CoA and its possible effect on fatty acid oxidation. *Arch. Biochem. Biophys. 298*, 527–531.
37. He, X. Y., Yang, S. Y., and Schulz, H. (1989) Assay of L-3-hydroxyacyl-coenzyme A dehydrogenase with substrates of different chain lengths. *Anal. Biochem. 180*, 105–109.
38. Tolia, N. H., and Joshua-Tor, L. (2006) Strategies for protein co-expression in Escherichia coli. *Nat. Methods 3*, 55–64.